

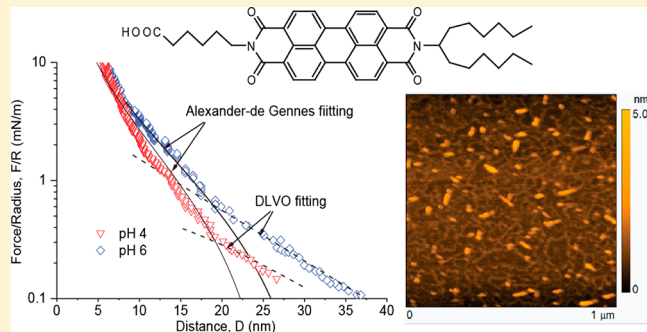
# Molecular Interactions of a Polyaromatic Surfactant C5Pe in Aqueous Solutions Studied by a Surface Forces Apparatus

Jing Wang,<sup>†</sup> Qingye Lu,<sup>†</sup> David Harbottle,<sup>†</sup> Johan Sjöblom,<sup>‡</sup> Zhenghe Xu,<sup>\*,†</sup> and Hongbo Zeng<sup>\*,†</sup>

<sup>†</sup>Department of Chemical and Materials Engineering, University of Alberta, Edmonton, Alberta, T6G 2V4 Canada

<sup>‡</sup>Ugelstad Laboratory, Department of Chemical Engineering, Norwegian University of Science and Technology (NTNU), N-7491 Trondheim, Norway

**ABSTRACT:** Studies on molecular mechanisms of polyaromatic surfactants in stabilizing water-in-oil (W/O) or oil-in-water (O/W) emulsions are of great scientific and practical importance. A polyaromatic surfactant *N*-(1-hexylheptyl)-*N'*-(5-carboxylicpentyl) perylene-3,4,9,10-tetracarboxylic bisimide (C5Pe) with well-defined molecular structure containing fused aromatic rings and heteroatoms similar to asphaltene molecules, was used in this study in an attempt to understand molecular interaction mechanisms of heavy oil components in aqueous solutions. A surface forces apparatus (SFA) was used to directly measure the molecular interactions of C5Pe. Solution pH, salt concentration and  $\text{Ca}^{2+}$  addition showed a strong impact on molecular interactions between C5Pe adsorbed on mica surfaces. The repulsion observed between the two adsorbed C5Pe molecular layers was shown to have a steric and electrostatic origin. The force-distance profiles at short separation distances under high compression force were well fitted with the Alexander-de Gennes (AdG) model. At pH  $\geq 4$ , the repulsive forces measured over a long separation distance under low compression force were shown to deviate from the AdG model but could be fitted with the Derjaguin-Landau-Verwey-Overbeek (DLVO) theory, indicating an electrostatic origin of the observed repulsion due to ionization of  $-\text{COOH}$  groups. Adhesion between two C5Pe surfaces was shown to decrease sharply with increasing solution pH and salt concentration, being attributed to the decrease in surface hydrophobicity and hence hydrophobic attraction. Addition of  $\text{Ca}^{2+}$  ions induced the formation of large C5Pe aggregates due to strong bonding of  $\text{Ca}^{2+}$  with  $-\text{COOH}$  groups, leading to a longer range steric repulsion. Our results provide a new insight into the molecular interactions of polyaromatic surfactants at oil–water interfaces and in complex aqueous solutions.



## INTRODUCTION

Surfactants or amphiphiles are widely applied as cleaning, wetting, dispersing, foaming, and antifoaming agents in numerous practical applications of heterogeneous and/or multiphase systems, including detergents, paints, inks, cosmetics, firefighting fluids, food products, pesticides, etc. Surfactants are usually organic compounds containing both a hydrophilic headgroup and hydrophobic tail.<sup>1</sup> Therefore, a surfactant molecule can migrate to an air/water or oil/water interface where its tail extends out of the bulk aqueous phase, either into the air, or into the oil phase. As a consequence the surface tension of a liquid or the interfacial tension of two immiscible liquids is reduced from the pure liquid systems. The buildup of a monolayer and subsequent multilayers at the oil/water interface has immense importance in stabilization of emulsion systems.<sup>2–4</sup>

The formation and stabilization of emulsions are important in many industrial applications and processes. For example, oil-in-water (O/W) emulsions are commonly encountered in food processing and products, such as homogenized milk, mayonnaise, and cream in espresso.<sup>5,6</sup> In medicine, microemulsions are used to deliver vaccines and kill microbes.<sup>7</sup> In these cases,

stable emulsions are intentionally formulated. Stable emulsion systems are also often used for synthesis of functional materials and polymeric materials. Alternatively, demulsification by coalescence of oil or water droplets is sometimes more desirable. For instance, in the processing of oil sands, problematic stable emulsions form during bitumen extraction and bitumen froth treatment. In the latter case, emulsions are water-in-oil (W/O) with trapped water having to be removed to produce a bitumen product that contains minimal water. This is desirable as the trapped water containing dissolved salts (e.g.,  $\text{Cl}^-$ ) will lead to corrosion issues in downstream processing equipment.<sup>8</sup> Water removal is often achieved through the addition of demulsifiers that disrupt interfacial protecting films to promote droplet coalescence, which in turn enhances separation through gravity separation. On the other hand, tiny bitumen droplets in the form of bitumen-in-water emulsions can form during bitumen extraction, which leads to a reduced recovery of bitumen and causes many challenging

Received: May 8, 2012

Revised: July 17, 2012

Published: August 22, 2012

issues in tailings treatment.<sup>8,9</sup> The presence of naturally occurring amphiphilic compounds, e.g., polycyclic aromatic surfactants (asphaltenes and naphthenic acids), positioned at the O/W interface has been shown to have a significant impact on the stability of these undesirable W/O or O/W emulsions.<sup>10–14</sup>

Asphaltenes are a class of compounds in crude oil that are defined not by a uniform molecular structure but as a solubility class.<sup>15–17</sup> Asphaltenes are generally accepted as polycyclic aromatic and amphiphilic compounds composed of condensed aromatic rings with alkyl chains attached.<sup>18–22</sup> The polarity of asphaltenes mainly arises from acidic, thiophenic, and hydroxylic functional groups. Due to their complex structures and chemical compositions, the molecular interactions of asphaltenes and their roles in various interfacial and fouling phenomena remain largely unknown, despite recent measurements of molecular forces using atomic force microscope (AFM) and surface forces apparatus (SFA).<sup>8,18,19,23–25</sup> Investigating the molecular interactions and interfacial properties of asphaltene model compounds with well-defined chemical structures has been considered as a necessary step in developing a better understanding of the complex molecular interaction mechanisms of asphaltenes in organic solvents and aqueous solutions.<sup>26</sup>

Recently, several polycyclic aromatic surfactants have been synthesized as asphaltene model compounds by attaching hydrophobic branch(es) to one end and alkyl chain(s) of different polar groups to the other end of a perylene core.<sup>27–29</sup> Using several complementary techniques, Nordgard et al. showed that the polycyclic aromatic surfactants were able to stabilize both W/O and O/W emulsions.<sup>27–29</sup> It was also shown that the oil/water interfacial tension decreases sharply with the addition of these polycyclic aromatic surfactants, depending on the concentration of the surfactant in organic phase and pH or divalent cation concentration of solutions.<sup>27–29</sup>

The objective of this study is to elucidate the molecular interaction mechanisms of a polycyclic aromatic surfactant *N*-(1-hexylheptyl)-*N'*-(5-carboxylicpentyl) perylene-3,4,9,10-tetracarboxylic bisimide (C5Pe; Figure 1a) in aqueous solutions. C5Pe consists of four aromatic rings fused together with three cyclic rings containing heteroatoms O and N. One end of the fused rings is attached with a pentyl carboxylic acid via the nitrogen atom, and the other end is connected to a hexyl-heptyl double chain also through a nitrogen atom. The polycyclic structure and amphiphilic nature of C5Pe, although simplified, fall into the well-accepted asphaltene structure and nature.<sup>22,30,31</sup> However, it is noted that a single polycyclic aromatic surfactant is unlikely to mimic quantitatively the aggregation of complex asphaltenes in a given solvent. As C5Pe has a –COOH terminal group, the solution conditions such as pH, salinity, and Ca<sup>2+</sup> addition are expected to show a significant impact on the molecular forces and interfacial behavior of C5Pe. In this study, the forces between adsorbed C5Pe surfaces on mica were measured in aqueous solutions using a surface forces apparatus (SFA), which allows accurate and direct determination of forces between two surfaces as a function of absolute separation distance with force sensitivity down to ~10 nN and distance resolution of ~0.1 nm.<sup>32–34</sup> The results obtained from this study provide a new insight into the molecular interaction mechanisms and interfacial properties of polycyclic aromatic surfactants in various oil–water systems.

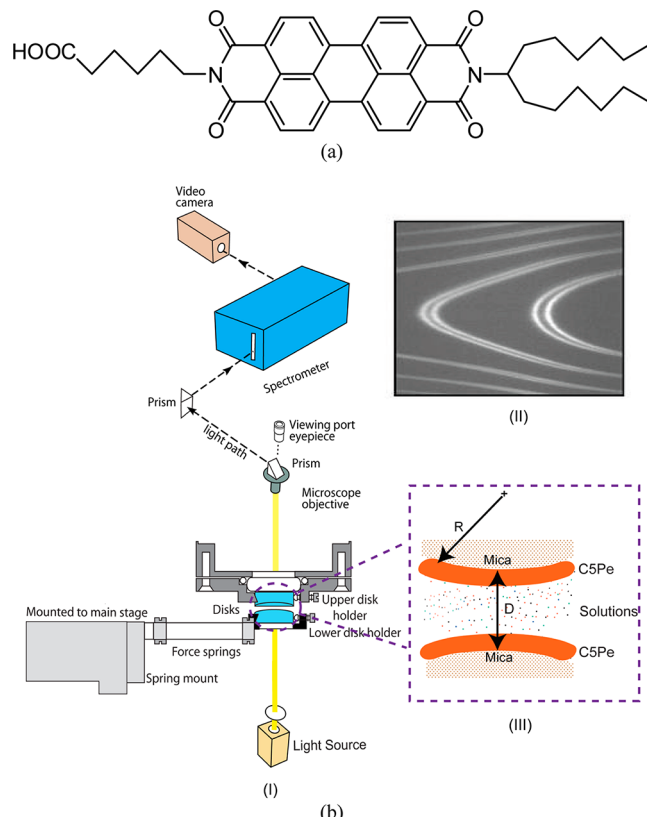


**Figure 1.** (a) Molecular structure of polycyclic aromatic surfactant C5Pe (MW = 689) with nomenclature *N*-(1-hexylheptyl)-*N'*-(5-carboxylicpentyl) perylene-3,4,9,10-tetracarboxylic bisimide. (b) Schematic of SFA experimental setup for studying the surface interactions of C5Pe.

## MATERIALS AND EXPERIMENTAL METHODS

**Materials.** Details on the synthesis of C5Pe were reported previously.<sup>28</sup> C5Pe stock solutions were prepared in HPLC grade toluene (>99.9%, Fisher Scientific, Canada). To ensure complete dissolution of C5Pe, a 0.2 mM C5Pe-in-toluene stock solution was sonicated for 30 min, left for more than 24 h, and filtered using a 0.2 µm filter before its use. All other chemicals were purchased from Fisher Scientific Canada and used as received, unless otherwise specified.

**Film Preparation.** The C5Pe films were prepared by adsorption method as reported recently.<sup>8</sup> Briefly, several drops of C5Pe solution were placed on a thin mica sheet which was glued on a cylindrical silica disk with radius of R = 2 cm. The C5Pe was allowed to adsorb for 5 min in a sealed chamber saturated with toluene vapor, forming a film that was subsequently washed by pure toluene. To obtain a more compact film, the adsorption process was repeated for at least 3 times. After further washing by pure toluene, the C5Pe film on mica was loaded into the SFA chamber and used for the force measurements by SFA and topographic imaging by AFM.

**Force Measurement (SFA).** An SFA (SurSurface LLC, Santa Barbara, CA, USA) was used to measure the interaction forces of C5Pe in aqueous solutions. Due to its unique ability to simultaneously measure the force, F, as a function of the absolute separation distance, D, and the local geometry of two interacting surfaces (the local radius R or contact area), SFA has been extensively used to determine the molecular interactions in many biological and nonbiological systems *in situ* and *in real time*.<sup>32,34–36</sup> The working principle of SFA and

detailed experimental setup were reported previously.<sup>33,40–43</sup> A typical SFA is shown schematically in Figure 1b. Briefly, a thin piece of mica sheet ( $1\text{--}5\ \mu\text{m}$ ) was glued on a cylindrical silica disk ( $R = 2\ \text{cm}$ ), and a layer of C5Pe was adsorbed/coated on the exposed mica surface. The two prepared disks were then mounted into the SFA chamber in a cross-cylinder geometry, which corresponds to a sphere of radius  $R$  approaching a flat surface when the separation of the two surfaces is much smaller than its radius  $R$ .<sup>44</sup> The absolute separation distance between the two surfaces,  $D$ , was determined by an optical technique called multiple beam interferometry (MBI) using interference fringes of equal chromatic order (FECO) (Figure 1b (II)). The distance measured as such could be down to a resolution of  $\sim 0.1\ \text{nm}$ . The force  $F(D)$  was determined as a function of the separation distance  $D$  based on the deflection of the supporting double cantilever spring. The measured force,  $F(D)$ , can be converted into energy per unit area between two flat surfaces  $W(D)$  by the Derjaguin approximation:  $F(D) = 2\pi R W(D)$ .<sup>44</sup> When  $\partial F(D)/\partial D$  is greater than the stiffness of spring, there is a mechanical instability that causes the lower surface to jump either toward or away from the upper surface during approaching or retracting process, respectively. The experimental configuration for measuring the interactions between two C5Pe surfaces in an aqueous solution is shown in Figure 1b (III).

**Langmuir–Blodgett (LB) Trough Experiments and Deposition.** Interfacial pressure–area isotherms of C5Pe were obtained using a Langmuir interfacial trough (KSV Instruments, Finland) with an effective trough area of  $17\,010\ \text{mm}^2$ . Prior to their use the trough and barriers were thoroughly cleaned successively with toluene, acetone and ultrapure water of resistivity  $18.2\ \text{M}\Omega\ \text{cm}$ . To form an interfacial film of C5Pe,  $50\ \mu\text{L}$  of  $0.2\ \text{mM}$  C5Pe-in-toluene solution was first spread on an ultrapure water subphase. After a 10-min incubation period,  $100\ \text{mL}$  optima toluene was poured carefully over the aqueous phase to form an organic top phase. After 30 min equilibration, compression and expansion of the interfacial film was carried out by moving both barriers inward and outward at a speed of  $5\ \text{mm}/\text{min}$ . The compression–expansion cycle was conducted one after another without interruption for 3 times.

Hydrophilic silicon wafers were cleaned with Piranha solution using a reported procedure<sup>45</sup> and used for LB film deposition. The cleaned silicon wafer was first immersed completely into the water subphase with the flat surface placed parallel to the barrier before spreading the C5Pe film on the water subphase. The C5Pe layer prepared using the procedures described above was then compressed to a predetermined interfacial pressure. The interfacial pressure was held constant while pulling the substrate up through the toluene–water interface, transferring the C5Pe film onto the substrate. The C5Pe film formed as such is referred to as LB film.

**AFM Imaging.** Morphology of C5Pe layer adsorbed or deposited on mica was characterized by an Agilent 5500 AFM (Agilent Technologies, Inc., Chandler, AZ), operated under acoustic AC mode in air. Silica cantilevers (RTESP, Veeco, Santa Barbara, CA) with a nominal resonance frequency of  $200\text{--}400\ \text{kHz}$  were used for imaging. The resonance frequency of a cantilever was obtained by “auto tuning” in the AFM software. Phase imaging was performed simultaneously along with topography imaging. During imaging, the amplitude set point ( $A_s$ ) was set at 98% of the free amplitude ( $A_0$ ). With such set point, the tapping force between the cantilever tip and the

sample surface is sufficiently small that damage to the film by the scanning tip is negligible.

**Zeta Potential.** Zeta potential of C5Pe aggregates was measured using a zeta potential analyzer (Brookhaven Instruments Corp. ZetaPALS, NY, USA). Since the C5Pe compound was not readily to disperse in water, 4 droplets of ethanol were placed onto the dry sample and left to evaporate for one hour to aid the dispersion of C5Pe in  $1\ \text{mM}$  KCl electrolyte solution. A suspension was prepared to  $0.015\ \text{wt.\%}$  of C5Pe in electrolyte solutions and sonicated for 5 min prior to zeta potential measurement. Zeta potentials were measured as a function of pH, with pH adjustments made using a complementary acid (HCl) and base (KOH).

## RESULTS AND DISCUSSION

**Characterization of C5Pe Film.** AFM images of molecularly smooth mica surface without and with adsorbed C5Pe film are shown in Figure 2. As expected, freshly cleaved

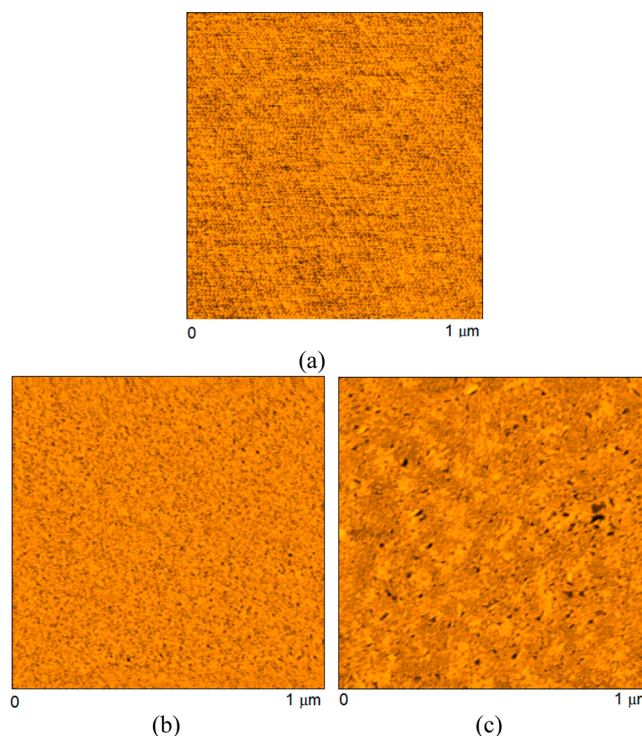


**Figure 2.** AFM images of (a) bare mica surface (vertical scale is from 0 to  $0.3\ \text{nm}$ ), (b) C5Pe adsorbed on mica (vertical scale is from 0 to  $1.2\ \text{nm}$ ), and (c) C5Pe adsorbed on mica after immersing in pH 2,  $10\ \text{mM}$  KCl solution for 10 min (vertical scale is from 0 to  $2.0\ \text{nm}$ ).

mica is featureless and flat with a root-mean-square (rms) roughness<sup>46,47</sup> of  $0.2\ \text{nm}$  (Figure 2a). In contrast, the adsorbed C5Pe film is much rougher with a rms roughness of  $0.5\ \text{nm}$ .

To study the effect of the exposure of adsorbed C5Pe to aqueous solutions on their configuration on mica surface, the adsorbed C5Pe film was immersed in electrolyte aqueous solutions for 10 min and dried in air in a dust-free laminar flow hood. The AFM image in Figure 2c shows a further increase in rms roughness from  $0.5$  to  $1.3\ \text{nm}$  after immersion of the adsorbed C5Pe film in  $10\ \text{mM}$  KCl solution at pH 2. It is interesting to note the formation of C5Pe aggregates on the film after exposure to the aqueous solution. During film preparation, C5Pe was adsorbed onto hydrophilic mica through

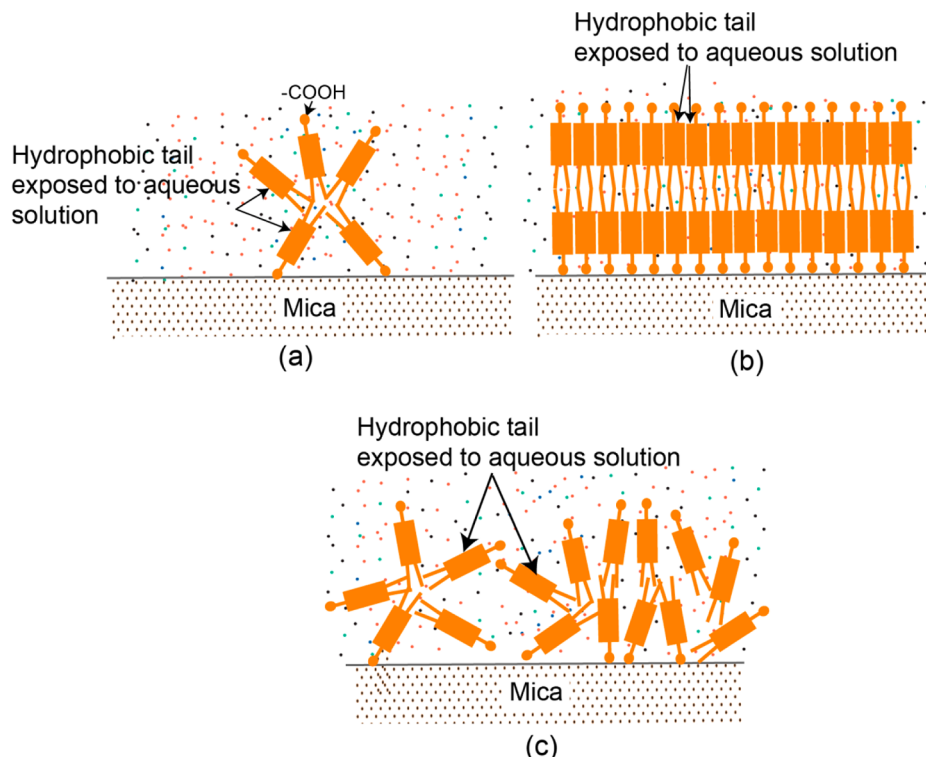


**Figure 3.** Proposed schematic of C5Pe aggregates on mica surfaces: (a) micelle-like aggregates, (b) an ordered bilayer structure and (c) complex aggregates combining micelle-like and “multilayer” aggregation.

hydrogen bonding, leading the hydrophobic tails most likely facing the toluene. After exposure of the film to an aqueous solution, some of the hydrophilic head groups could flip so that they are exposed to the more favorable aqueous phase. Due to its large hydrophobic group and small hydrophilic headgroup, the C5Pe molecules were unable to form a uniform monolayer or bilayer; instead, they form micelle-like aggregates after exposure to low pH aqueous solutions. As a result, the hydrophobic groups tend to stay inside the aggregate and the hydrophilic  $-COOH$  groups expose to both the aqueous solutions and mica surface, as shown schematically in Figure 3.

The Langmuir isotherm is often used to study molecular state and mechanical properties of an interfacial film. Figure 4 shows the typical interfacial pressure-area ( $\pi$ - $A$ ) isotherms of C5Pe at a toluene–water interface. It is interesting to note the absence of a clear phase transition for a C5Pe interfacial film, qualitatively similar to interfacial isotherms of asphaltenes.<sup>17</sup> A clear hysteresis in the  $\pi$ - $A$  isotherm was observed between the first and second compressions, with the second compression exhibiting a much lower interfacial pressure at a given trough area. Although some C5Pe may have transferred from the interface into the top toluene phase under compression, the observed hysteresis is mostly likely due to the enhanced molecular aggregation of C5Pe under pressure. If the molecular transfer from the toluene–water interface into the toluene top phase was the main cause for the observed hysteresis, one would expect recovery of  $\pi$ - $A$  isotherm provided an extended incubation time being given. To test this hypothesis, a third compression was conducted after the film was incubated for 3 h. No further hysteresis between the second and third compression was observed, clearly indicating the irreversible nature of molecular aggregation at the toluene–water interface during the first compression. For C5Pe molecules, the  $\pi$ - $\pi$  interactions among polyaromatic rings and hydrophobic

interactions of linear hydrocarbon tails are considered as the main driving forces for C5Pe aggregation at the toluene–water interface. A typical AFM image of a C5Pe LB film deposited at a constant interfacial pressure of 5 mN/m with a pulling speed of 1 mm/min in Figure 4 confirms molecular aggregation of C5Pe at the toluene–water interface. It is interesting to note a nonuniform film of C5Pe aggregates on the silicon substrate. The C5Pe aggregates with average size of  $\sim$ 50 nm in diameter were seen across the surface.

**Surface Forces Measurements and Analysis.** Figure 5a shows a typical force–distance profile for two adsorbed C5Pe surfaces approaching each other in a 1 mM KCl solution at pH 2, and Figure 5b shows the force profile for separation. The hard wall distance is determined to be  $\sim$ 5.8 nm (note that the “hard wall” distance in this study is defined as the mica–mica separation distance or thickness of confined C5Pe, which changed little with increasing the normal load or pressure). A repulsive force was first measured between the two surfaces at distances  $D > 9$  nm, followed by a jump-in at  $D \sim 9$  nm, to the hard wall separation distance. The observed repulsion could be arisen from electrostatic repulsion if C5Pe is charged at this pH. To confirm whether this repulsion is indeed from electrostatic repulsion, the zeta potential of C5Pe in simple electrolyte solution was measured. The results in Figure 6b show a negligible charge of C5Pe at this pH, suggesting a different origin of the observed repulsion.

In order to understand the surface forces measured, the measured force profile is further analyzed and discussed as follows. At pH 2, the Derjaguin–Landau–Verwey–Overbeek (DLVO) interaction (sum of van der Waals (vdW) force and electrostatic double layer force) is not significant based on the considerations as follows. (1) The above zeta potential measurement shows that the zeta potential of C5Pe aggregates dispersed is around zero, indicating that C5Pe surface is nearly

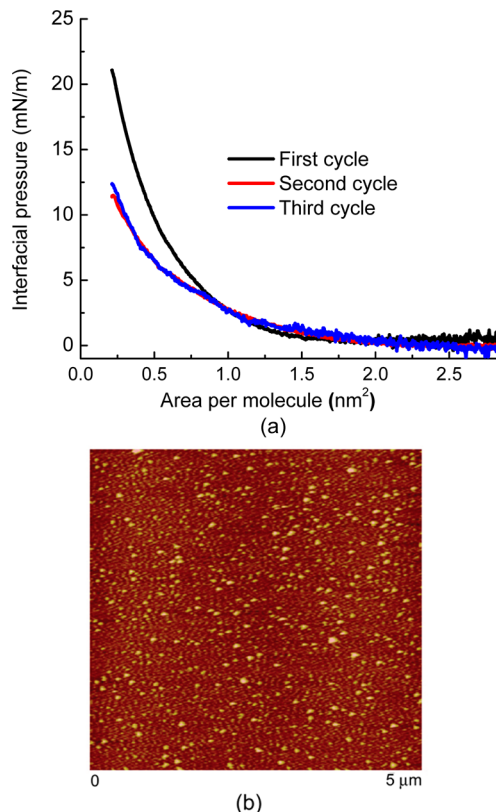


**Figure 4.** (a) Interfacial pressure–area isotherms of C5Pe film at toluene–water interface obtained with an interfacial Langmuir–Blodgett (LB) trough, in which the second cycle was carried out immediately after the first compression, and the third cycle was carried out 3 h after the second compression; (b) AFM image (vertical scale is from 0 to 5.0 nm) of C5Pe film deposited using LB method at an interfacial pressure of 5 mN/m at a pulling speed of 1 mm/min during the first cycle with a transfer ratio of 1.15.

neutral under the solution condition investigated. (2) Although mica is charged if it is exposed directly to the solution, the mica is mostly covered by C5Pe molecules (as shown in the AFM images) which should not carry significant charge. As the vdw force and electrostatic double layer force are mainly determined by the properties of interacting surfaces, the interactions between the mica substrates underneath the coated C5Pe layers should be negligible. (3) It should be noted that due to the conformation change and aggregation of C5Pe molecules part of the mica substrate might be exposed to water leading to mica “patches”. However, the DLVO forces arising from these small “charged” exposed mica patches would be much weaker than the repulsive forces measured because of the high surface coverage of C5Pe. The 52° water contact angle on C5Pe surface at pH 2 was mainly due to the hydrated  $-COOH$  group facing water phase (and might be also due to these mica patches). It should be also noted that analysis of DLVO interactions between two rough surfaces with inhomogeneous charges is a challenging issue in the field of colloid and interface science which is out of the scope of the current study (for example, surface element integration method was used recently to analyze the DLVO forces to account for the surface roughness<sup>48</sup>). It was reported recently that steric interactions between two asphaltene layers or two C5Pe layers in organic solvents could be described by the Alexander–de Gennes (AdG) model for polymer brush layers.<sup>8,23</sup> While two C5Pe

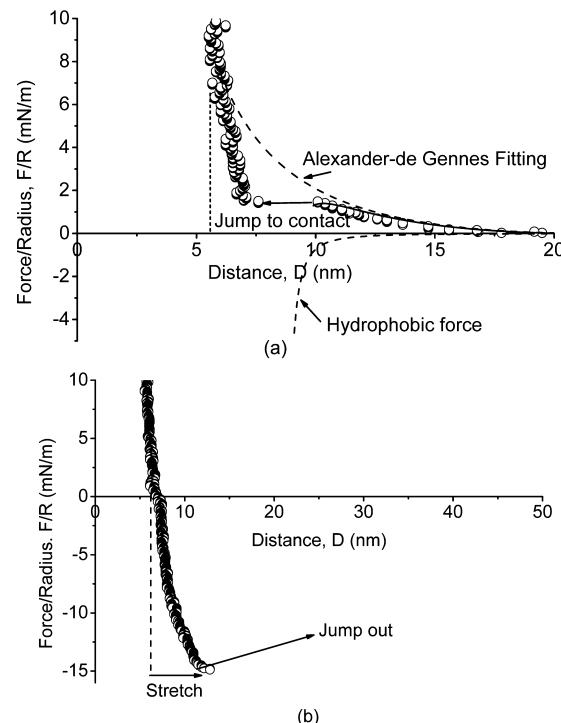


**Figure 5.** Force–distance profiles of two C5Pe surfaces interacting in 1 mM KCl solution at pH 2: (a) approach force curve; (b) retraction force curve following the approach (a). Open squares are the measured force profile; solid curve is the fitted curve by combining AdG theory with a fitted  $L$  of 10 nm and  $s$  of 6.6 nm and hydrophobic force with a fitted  $K$  of  $1.0 \times 10^{-20}$  J. Dashed curves in panel a are fitted curves by AdG theory and hydrophobic force, respectively.

layers cannot be considered as two polymeric brushes due to the small molecular weight, and water is not a good solvent for C5Pe, the C5Pe aggregates and their interesting conformation may lead to steric interactions between the two surfaces in aqueous solutions. The aggregates may bear some brush properties which could be described by the AdG model.<sup>49</sup> In the AdG model, as two surfaces approach each other, the films start to overlap at a certain distance, leading to an increase in local density of molecular segments. The increased local density of molecular segments leads to an increase in osmotic pressure and repulsive interaction energy. The repulsive pressure between two planar surfaces is given by eq 1<sup>44</sup>

$$P(D) \approx \frac{kT}{s^3} \left[ \left( \frac{2L}{D} \right)^{9/4} - \left( \frac{D}{2L} \right)^{3/4} \right] \quad \text{for } D < 2L \quad (1)$$

where  $P(D)$  is the repulsive pressure between the two C5Pe films ( $N/m^2$ ),  $k$  is Boltzmann constant ( $m^2 kg/s^2/K$ ),  $T$  is temperature (K),  $s$  is the average space (m) between two “grafting” points of the molecules, and  $L$  is brush layer thickness (m). For the geometry of two crossed cylindrical surfaces of radius  $R$ , the force–distance relation  $F(D)$  can be derived by integrating eq 1 using the Derjaguin approximation<sup>50</sup> as shown in eq 2.

$$\frac{F(D)}{R} = \frac{16\pi kT L}{35s^3} \left[ 7 \left( \frac{2L}{D} \right)^{5/4} + 5 \left( \frac{D}{2L} \right)^{7/4} - 12 \right] \quad \text{for } D < 2L \quad (2)$$

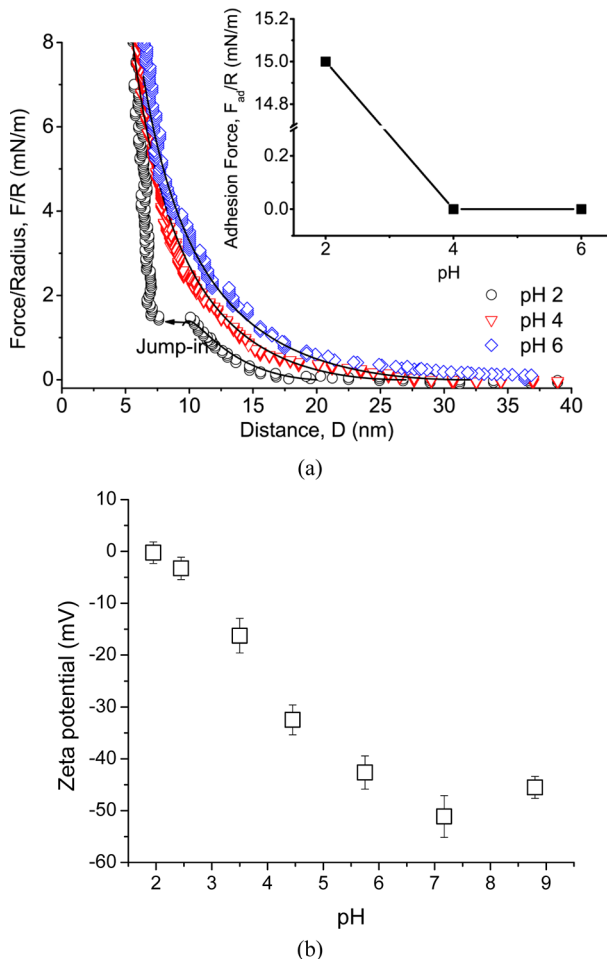


**Figure 6.** (a) Force–distance profiles of two C5Pe surfaces interacting in 1 mM KCl solution at different pH during approach. Solid curves are fitted results using the AdG model with the fitted values: (I) pH 2,  $L = 10$  nm,  $s = 6.6$  nm; (II) pH 4,  $L = 13.5$  nm,  $s = 7.3$  nm; (III) pH 6,  $L = 16$  nm,  $s = 8.1$  nm. Inset is the adhesion measured during separation. (b) Zeta potentials of C5Pe aggregates dispersed in 1 mM KCl electrolyte solution.

As shown in Figure 5a (and Figure 6a for pH 2), the repulsive force at  $D > 9$  nm can be well fitted with the AdG equation with the fitted  $L$  and  $s$  being 10 and 6.6 nm, respectively, indicating that the repulsive surface force measured at pH 2 can well be resulting from an additional interaction component, i.e., steric interaction well described by the AdG model. However, the jump-in motion at  $D \sim 9$  nm must be due to some strong attractive force which cannot be predicted by the steric interaction based on the AdG equation. This additional attractive force could most likely be the hydrophobic forces between the two C5Pe films. C5Pe is constituted by a small hydrophilic headgroup ( $-COOH$ ) and a long hydrophobic tail as shown in Figure 1a. Geometrically, it is almost impossible that the hydrophilic headgroup could fully shield and prevent the exposure of large hydrophobic groups to water even in the most hydrophilic configuration as shown in Figure 4b. Thus the hydrophobic tails exposed to the aqueous solution can form local hydrophobic domains and induce hydrophobic forces between the two C5Pe films.<sup>51</sup> The hydrophobic surface forces  $F_{HB}$  can be approximately described by an empirical equation shown in eq 3, where  $K$  is a fitted value (J), representing the strength of hydrophobic interaction

(similar to the Hamaker constant for van der Waals forces), and  $D_0$  is the fitted hard wall distance of the measured force–distance profiles.<sup>44</sup>

$$\frac{F_{HB}}{R} = -\frac{K}{6(D - D_0)^2} \quad (3)$$

As shown in Figure 5a, the force–distance curve and the jump-in could be well fitted by including the hydrophobic force with fitted  $K$  and  $D_0$  of  $1 \times 10^{-20}$  J and 6.8 nm, respectively. Figure 5b shows the force–distance profile obtained when the two C5Pe surfaces were separated after being kept in contact for 1 min following the approach to contact in Figure 5a. A strong adhesion  $F_{ad}/R$  of  $\sim 15$  mN/m was measured, which was mainly due to the attractive hydrophobic interaction between the hydrophobic domains of the interacting films. Interestingly, the two surfaces were stretched for about 6 nm before detachment (jump apart) as shown in Figure 5b, which indicates a stretch of each film by  $\sim 3$  nm. The extended length of C5Pe molecules was estimated to be 2.7 nm based on molecular configuration of C5Pe molecule, the bond lengths of C–C ( $SP^3$ – $SP^3$ ), C–N, C–O, and C–C (benzene) to be 0.15, 0.14, 0.14, and 0.14 nm, respectively, and the bond angle to be  $109.5^\circ$ ,  $180^\circ$ ,  $180^\circ$ , and  $120^\circ$ , respectively.<sup>52,53</sup> The actual molecular length of C5Pe should be smaller than 2.7 nm. The stretching associated with separation shown in Figure 5b confirms that C5Pe molecules aggregate on mica surface upon exposure to aqueous environment, as also visualized by AFM imaging. The above results from the force measurement indicate the molecular interactions of C5Pe in aqueous solution being largely affected by the aggregation of the polyaromatic molecules, due to  $\pi$ – $\pi$  interactions among aromatic rings and hydrophobic interactions. It is expected that the solution conditions, such as pH, salinity and presence of  $Ca^{2+}$ , can significantly impact the molecular interactions of C5Pe, which will be discussed in great detail below.

**Effect of pH.** The interaction forces between two C5Pe surfaces in 1 mM KCl solution as a function of pH were measured. The results in Figure 6 show a strong impact of pH on measured forces as anticipated. At pH 2, repulsive forces were measured at  $D > 9$  nm followed by a jump-in at  $D \approx 9$  nm under a soft compression, as discussed in detail above. With increasing pH to 4, only monotonic repulsive forces without jump-in were observed. When pH was further increased to 6, the repulsive forces became stronger and longer ranged than that at pH 4. The absence of an adhesive jump-in at pH higher than 2 was attributed to the decreased hydrophobicity, a result of increased ionization of carboxylic acids on C5Pe with increasing pH. Considering  $pK_a$  of C5Pe at approximately pH 6, such behavior is consistent with increasing measured zeta potential value at increasingly higher pH (more basic), i.e., more negatively charged, as shown in Figure 6b. At pH 2, the ionization or protonation of  $-COOH$  is negligible, making the surface of highest hydrophobicity. For a pair of hydrophobic surfaces in water, an adhesive jump-in is anticipated once they overcome a moderate repulsion during the approach of the two surfaces. At pH 4, sufficient ionization of the  $-COOH$  groups to  $-COO^-$  decreases the hydrophobicity of the C5Pe surface, inducing a stronger repulsion and causing the disappearance of hydrophobic adhesion. At pH 6, most of  $-COOH$  groups in C5Pe have been ionized to  $-COO^-$ , further increasing surface charge density and decreasing surface hydrophobicity. The increased concentration of  $-COO^-$  and decreased hydro-

phobicity of the surfaces resulted in a further increase in electrostatic repulsion. To confirm the change in hydrophobicity with pH, droplet contact angles were measured on CSPe surface using a KRÜSS DSA10 (KRÜSS, U.S.A.). With 1 mM KCl solution, contact angles of  $34^\circ \pm 1^\circ$  and  $52^\circ \pm 2^\circ$  were measured at pH 6 and 2, respectively. Increasing hydrophobicity with decreasing pH is in agreement with the force-profiles; confirming the nature of the jump-in at pH 2.

The logarithmic force-distance profiles at pH 4 and 6 in Figure 7 show that the AdG equation fits the force-distance

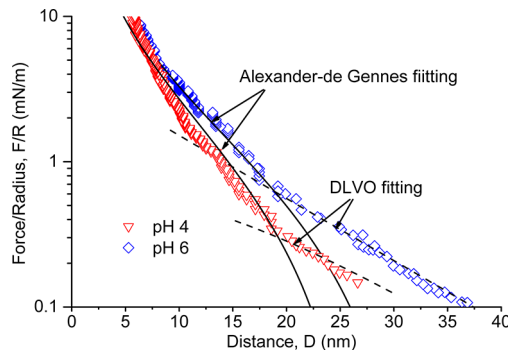


**Figure 7.** Force–distance profiles of two CSPe surfaces interacting in 1 mM KCl solution at pH 4 and 6. Solid curves are the fitted results by AdG model at short separation distance and high compression regime, and dashed curves are the fitted results using the DLVO theory at long separation distance and low compression regime with Hamaker constant  $A_{CWC} = 2.8 \times 10^{-21}$  J, and fitted decay lengths and surface potentials of (I) pH 4,  $\psi = -32$  mV,  $\kappa^{-1} = 9.8$  nm; (II) pH 6,  $\psi = -50$  mV,  $\kappa^{-1} = 9.8$  nm.

profiles well at short separation distance under a relatively high compression force, but deviates at longer separation distances and low compression forces. The forces predicted by a single AdG model at longer distance are smaller than the measured forces, indicating the presence of other repulsive forces at longer separation distances. This long-range repulsive force is most likely a result of the electrostatic repulsion from the negatively charged CSPe surfaces at pH 4 and 6 due to the ionization of  $-COO^-$  groups, as discussed above.

The classic DLVO theory describes the forces between two charged surfaces interacting in an aqueous medium. The total interaction force ( $F_{\text{total}}$ ) is the summation of van der Waals forces ( $F_V$ ) and electrostatic force ( $F_E$ ), as given in eq 4.<sup>51</sup>

$$F_{\text{total}} = F_V + F_E \quad (4)$$

The van der Waals forces between two crossed cylindrical surfaces of radius  $R$  are given in eq 5

$$\frac{F_V}{R} = -\frac{A_{CWC}}{(6D^2)} \quad (5)$$

where  $A_{CWC}$  is Hamaker constant for CSPe/Water/CSPe, taken to be  $2.8 \times 10^{-21}$  J in this study.<sup>18</sup> The electrostatic force for two identically charged particles can be calculated by numerically solving the Poisson–Boltzmann equation (eq 6) in the form of eq 7 for constant surface charge boundary conditions,<sup>20</sup> i.e., at  $x = 0$ ,  $(d\psi/dx)|_{x=0} = \text{constant}$ , and at  $x = \infty$  and  $\psi = 0$ .

$$\epsilon\epsilon_0 \frac{d^2\psi}{dx^2} = -e \sum_i z_i n_{i\infty} \exp\left(-\frac{z_i e \psi}{kT}\right) \quad (6)$$

$$\frac{F_E}{R} = -2\pi \left[ kT n_{i\infty} \sum_i \left( 1 - \exp\left(-\frac{z_i e \psi}{kT}\right) \right) - \frac{\epsilon\epsilon_0}{2} \left( \frac{d\psi}{dx} \right)^2 \right] \quad (7)$$

In eqs 6 and 7 above,  $\epsilon$  is the dielectric constant of aqueous solution and  $\epsilon_0$  is the permittivity of vacuum ( $C^2/N\cdot m^2$ ),  $e$  is elementary charge (C),  $z_i$  is the valence of  $i$ th ions,  $n_{i\infty}$  is the concentration of  $i$ th ion in bulk solutions (mol/L),  $k$  is the Boltzmann constant, and  $T$  is the temperature ( $T = 298$  K). The reciprocal decay length,  $\kappa$  is defined in eq 8 as

$$\kappa = \left( \frac{e^2}{\epsilon k T} \sum_i n_{i0} z_i^2 \right)^{1/2} \quad (8)$$

During the fitting, the surface potential  $\psi$  and decay length  $\kappa^{-1}$  were set as adjustable parameters. The dashed lines shown in Figure 7 are the fitted curve using the above DLVO model with  $\psi = -32$  mV,  $\kappa^{-1} = 9.8$  nm, and  $\psi = -50$  mV,  $\kappa^{-1} = 9.8$  nm for pH 4 and 6, respectively.<sup>18</sup> The fitted decay length of 9.8 nm is in close agreement with the theoretical decay length ( $\kappa^{-1} = 10.4$  nm) for 1 mM KCl electrolyte solutions calculated using eq 8. It is interesting to note that the best fitted Stern potential values of  $-32$  and  $-50$  mV are in good agreement with measured zeta potential values of  $-30$  and  $-50$  mV at pH 4 and 6, respectively, supporting the argument that this long-range repulsion is indeed a result of electrostatic repulsion of overlapping electrical double layers. Combining the DLVO forces at longer separation distance and steric force at shorter separation distance, the measured force–distance profiles can be well fitted by the theory, as shown in Figure 7. The excellent fit suggests that the electrostatic double layer repulsive force dominates at longer distance and low compression regime, while steric force plays a more important role at shorter separation distance and high compression regime.

The adhesion force measured during separation in solutions of different pH is shown in the inset of Figure 6. Strong adhesion ( $F_{\text{ad}}/R$ ) of  $\sim 15$  mN/m was observed in 1 mM KCl solution of pH 2. The adhesion disappeared at pH 4 and 6 due to the decreased attractive hydrophobic force and increased electrostatic repulsive force.

The molecular interactions of CSPe were also measured in 1 mM KCl solutions of pH 8 and 10. The force–distance curves were similar to that of pH 6 and no adhesion was measured, which indicates that the head groups of CSPe were already completely ionized at pH 6, leading to similar electrostatic repulsion and negligible hydrophobic attraction. The complete ionization of carboxylic acid groups at pH around 6 is supported by a near constant zeta potential values at pH above 6 as shown in Figure 6b.

**Effect of Salinity at pH above  $pK_a$ .** Ionic strength plays an important role in determining interactions of charged particles or droplets in aqueous solutions by affecting their interfacial properties and electric double layers. The interaction forces between two CSPe surfaces at pH 6 were measured as a function of KCl concentration. The measured force–distance curves during approach are shown in Figure 8. With increasing KCl concentration from 1 mM to 100 mM, the range of the repulsive forces before reaching the hard wall separation became increasingly shorter, as a result of the electric double layer compression at higher salt concentrations. All the force–distance curves can be well fitted with the extended DLVO theory by including steric repulsion of the AdG equation. At

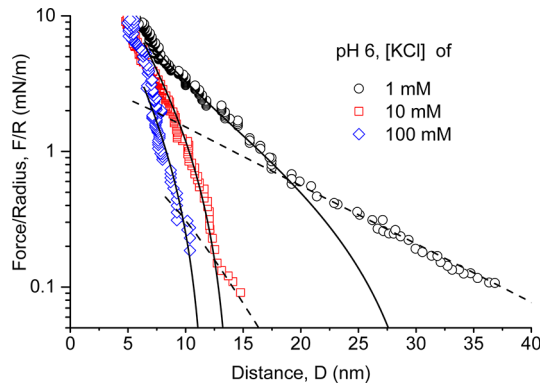


**Figure 8.** Force–distance profiles of two CSPe surfaces interacting in aqueous solutions of pH 6 with different KCl concentrations during approach. Solid curves are fitted results using AdG model with fitted parameters as: (I) for  $[KCl] = 1 \text{ mM}$ ,  $L = 16 \text{ nm}$ ,  $s = 8.1 \text{ nm}$ , (II) for  $[KCl] = 10 \text{ mM}$ ,  $L = 7.1 \text{ nm}$ ,  $s = 3.8 \text{ nm}$ , and (III) for  $[KCl] = 100 \text{ mM}$ ,  $L = 6 \text{ nm}$ ,  $s = 3.9 \text{ nm}$ ; dashed curves are the fitted results using DLVO theory with Hamaker constant  $A_{CWC} = 2.8 \times 10^{-21} \text{ J}$  and fitted decay lengths and surface potentials as: (I) for  $[KCl] = 1 \text{ mM}$ ,  $\varphi = -50 \text{ mV}$ ,  $\kappa^{-1} = 9.8 \text{ nm}$ ; (II) for  $[KCl] = 10 \text{ mM}$ ,  $\varphi = -20 \text{ mV}$ ,  $\kappa^{-1} = 3.3 \text{ nm}$ . In 100 mM KCl solution, the DLVO force is negligible compared to the strong steric force.

$[KCl] = 1 \text{ mM}$  and  $10 \text{ mM}$ , the fitted decay length of  $\kappa^{-1} = 9.8 \text{ nm}$  and  $3.2 \text{ nm}$  is in good agreement with theoretical values of  $\kappa^{-1} = 10.4 \text{ nm}$  and  $3.3 \text{ nm}$ , respectively, calculated using eq 8. At even higher salt concentration of  $[KCl] = 100 \text{ mM}$ , the electrical double layer was further suppressed ( $\kappa^{-1} \approx 1 \text{ nm}$ ), and the electrostatic contribution became negligible. Under this condition, the measured force profile can be fitted with a single AdG term as shown in Figure 8, suggesting dominating role of steric interactions.

**Effect of Salinity at pH below  $pK_a$ .** At pH 2, CSPe molecule is nearly neutral and the ionic strength is not expected to have a significant effect on the electric double layer forces. Figure 9a shows the force profiles of two CSPe surfaces in

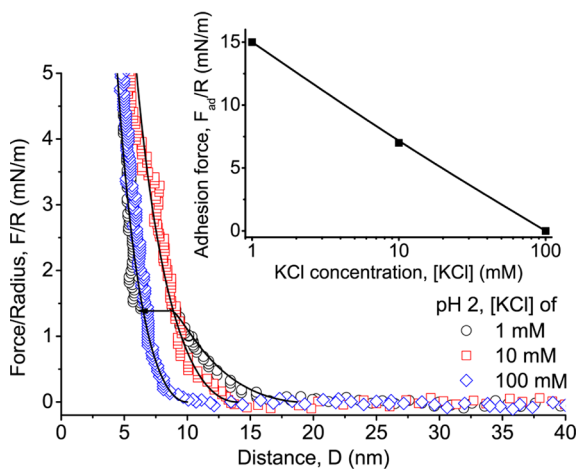


**Figure 9.** Force–distance profiles of two CSPe surfaces interacting in aqueous solutions of pH 2 of different KCl concentrations during approach. Solid curves are fitted results using the AdG model with fitted layer thickness and averaging spacing as: (I) for  $[KCl] = 1 \text{ mM}$ ,  $L = 10 \text{ nm}$ ,  $s = 6.6 \text{ nm}$ ; (II) for  $[KCl] = 10 \text{ mM}$ ,  $L = 7 \text{ nm}$ ,  $s = 4.3 \text{ nm}$ ; (III) for  $[KCl] = 100 \text{ mM}$ ,  $L = 5 \text{ nm}$ ,  $s = 3.7 \text{ nm}$ . Inset is the adhesion measured during the separation of two CSPe surfaces.

different KCl concentrations at pH 2. In this case, the range of interactions also decreased with increasing KCl concentrations from 1 to 100 mM, but to a much less extent as compared with the case at higher pHs. The force curves were fitted with the AdG equation by including hydrophobic force. The fitted film thickness  $L$  was 10, 7, and 5 nm, and the corresponding  $s$  was 6.6, 4.3, and 3.7 nm for the CSPe films in solutions of 1, 10, and 100 mM KCl concentrations, respectively. The hydrophobic force constant  $K$  also decreased from  $1.0 \times 10^{-20}$  to  $0.4 \times 10^{-20} \text{ J}$  with increasing KCl concentrations from 1 to 10 mM, leading to a weaker hydrophobic force. The hydrophobic force became negligible in 100 mM KCl solutions at pH 2. As shown in the inset of Figure 9a, the adhesion measured during the separation was  $F_{ad}/R = 15, 7, \text{ and } 0 \text{ mN/m}$  in 1, 10, and 100 mM KCl solutions, respectively. Since CSPe is considered nearly neutral at pH 2 as shown by near zero zeta potential values, the observed impact of increasing electrolyte concentration is likely due to its impact on hydrophobic forces between adsorbed CSPe molecules or aggregates with increasing electrolyte concentrations. It has been reported that increasing electrolyte concentration could reduce hydrophobic forces by weakening the structure of water molecules near hydrophobic entities.<sup>51,54,55</sup>

**Effect of  $\text{Ca}^{2+}$ .** Figure 10a shows the force–distance profiles of two CSPe surfaces approaching each other in 10 mM KCl solutions containing 0, 0.1, and 1 mM of  $\text{Ca}^{2+}$  at pH 2. It is interesting to note a significant increase in the hard wall distance from  $\sim 6 \text{ nm}$  to  $\sim 12 \text{ nm}$  and the disappearance of adhesion force as shown in the inset of Figure 10a with 0.1 mM

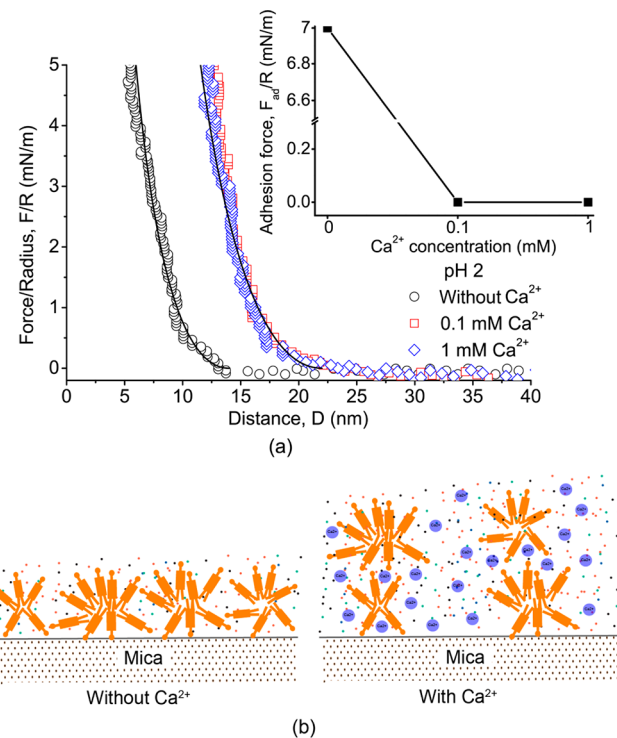


**Figure 10.** (a) Force–distance profiles of two CSPe surfaces interacting in 10 mM KCl solutions at pH 2 in the presence of different amount of  $\text{Ca}^{2+}$  ions. Solid curves are fitted results using the AdG model with fitted layer thickness and average spacing as: (I) without  $\text{Ca}^{2+}$ ,  $L = 7 \text{ nm}$ ,  $s = 4.3 \text{ nm}$ ; (II) with addition of 0.1 and 1 mM  $\text{Ca}^{2+}$ ,  $L = 11 \text{ nm}$ ,  $s = 4.2 \text{ nm}$ . (b) Proposed conformation change of CSPe molecules and aggregates in the presence  $\text{Ca}^{2+}$ .

$\text{Ca}^{2+}$  addition. The increased hard wall distance and the disappearance of adhesion were attributed to further aggregation of C5Pe induced by  $\text{Ca}^{2+}$  ions through bridging binding with the  $-\text{COOH}$  head groups. One  $\text{Ca}^{2+}$  ion is able to interact with two  $-\text{COOH}$  groups, bridging two small C5Pe aggregates into a large aggregate as shown in the schematics of Figure 10b, forming a bilayer of primary C5Pe aggregates. The presence of bilayer primary C5Pe aggregates accounts for a significantly increased hard wall distance. Similar impact of  $\text{Ca}^{2+}$  on the interaction of C5Pe surfaces was observed at higher pH as shown in Figure 11 for two C5Pe surfaces in the presence of 0 and 1 mM  $\text{Ca}^{2+}$  in 100 mM KCl solutions at pH 6.

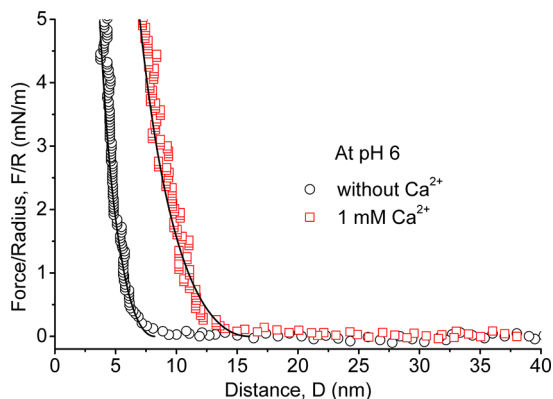


**Figure 11.** Force–distance profiles of two C5Pe surfaces interacting in 100 mM KCl solutions at pH 6 in the presence of different amount of  $\text{Ca}^{2+}$ . Solid curves are fitted results using AdG model with the fitted parameters as: (I) without  $\text{Ca}^{2+}$ ,  $L = 4 \text{ nm}$ ,  $s = 3.5 \text{ nm}$ ; (II) with 1 mM  $\text{Ca}^{2+}$  addition,  $L = 8 \text{ nm}$ ,  $s = 4.4 \text{ nm}$ .

Figure 12 shows AFM topography and phase images of adsorbed C5Pe film after immersion in 10 mM KCl solution

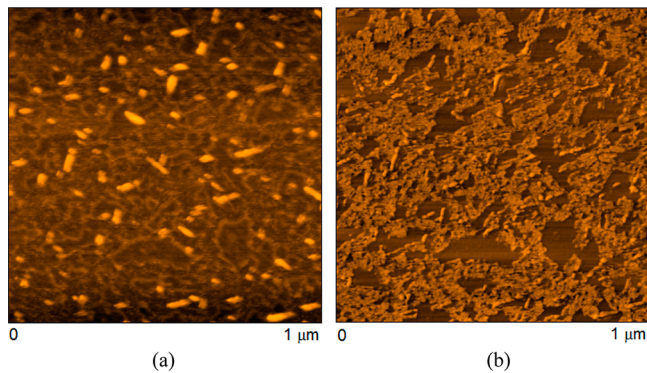


**Figure 12.** AFM images of a C5Pe film coated mica after immersing in aqueous solution of pH 2 with 10 mM KCl + 0.1 mM  $\text{CaCl}_2$  for 10 min: (a) topography (vertical scale is from 0 to 5.0 nm) and (b) phase images (vertical scale is from 0 to 22°).

containing 0.1 mM  $\text{CaCl}_2$  solution at pH 2 for 10 min. Compared with the C5Pe film immersed in 10 mM KCl solution without calcium ion addition (Figure 4), the C5Pe film forms much bigger aggregates with calcium ion addition. The rms roughness of C5Pe films increased from 1.3 to 3.6 nm with the addition of 0.1 mM calcium ions, representing an increase in film thickness by more than double. It is evident that the AFM images confirmed the proposed  $\text{Ca}^{2+}$ -induced aggregation mechanism.

## CONCLUSIONS

The molecular interactions of a polyaromatic surfactant C5Pe in aqueous solutions were directly measured by SFA. It was found that the interactions of C5Pe molecules were largely affected by solution pH, salt concentration and addition of  $\text{Ca}^{2+}$ . At high pH, the hydrophobicity of the adsorbed C5Pe film was decreased due to increased ionization of  $-\text{COOH}$  headgroup, thus lowering the attractive hydrophobic force. High electrolyte concentration compressed the electrostatic double layer and weakened hydrophobic forces of C5Pe surfaces, also leading to a significant reduction in adhesion. A small amount of  $\text{Ca}^{2+}$  ions in the aqueous solution were able to bridge two layers of primary C5Pe aggregates through its strong binding with  $-\text{COOH}$  groups, resulting in a much longer ranged steric repulsion and dramatically increased hard wall distance. The interactions of polyaromatic surfactant C5Pe in aqueous solution and organic solvents,<sup>26</sup> and asphaltene interactions in organic solvents<sup>8</sup> qualitatively agree with the recent molecular dynamics analysis,<sup>56</sup> that asphaltene can adsorb to mineral surfaces and self-aggregate under various solution conditions. However, it is noted that the simulation by Headen et al. was for interactions in vacuum (not in specific solvents).<sup>56</sup> It would be interesting to have more quantitative comparison between experimental measurements and theoretical simulations for polyaromatic surfactant molecules and surfaces in a range of solvents in future study. The results in the present study provide new insights into the fundamental molecular interactions of polyaromatic surfactants at oil–water interfaces and in complex aqueous solutions.

## AUTHOR INFORMATION

### Corresponding Author

\* (H.Z.) E-mail: hongbo.zeng@ualberta.ca. Phone: 780-492-1044. Fax: 780-492-2881. (Z.X.) E-mail: zhenghe.xu@ualberta.ca. Phone: 780-492-7667.

### Notes

The authors declare no competing financial interest.

## ACKNOWLEDGMENTS

The authors acknowledge an NSERC Discovery Grant Award and an NSERC RTI Grant Award for a Surface Forces Apparatus (SFA) (H.Z.), NSERC Industrial Research Chair Program in Oil Sands Engineering (Z.X.), and a grant from Statoil and financial support from Norwegian Research Council and Industry JIP1:2 consortium (J.S.) for the support of the study.

## REFERENCES

- (1) Rosen, M. J.; Kunjappu, J. T. *Surfactants and interfacial phenomena*, 4th ed.; Wiley: New York, 2012.
- (2) Becher, P. *Emulsions: theory and practice*; Reinhold: New York, 1957.
- (3) De Gennes, P. G.; Taupin, C. *J. Phys. Chem.* **1982**, *86*, 2294–2304.
- (4) Zettlemoyer, A. *J. Am. Chem. Soc.* **1958**, *80*, 3806–3806.
- (5) Kralova, I.; Sjöblom, J. *Surfactants used in food industry: A review*; Taylor & Francis: London, 2009; Vol. 30.
- (6) Xu, W.; Nikolov, A.; Wasan, D. T.; Gonsalves, A.; Borwankar, R. P. *J. Food Sci.* **1998**, *63*, 183–188.
- (7) Reed, S. G.; Bertholet, S.; Coler, R. N.; Friede, M. *Trends Immunol.* **2009**, *30*, 23–32.
- (8) Natarajan, A.; Xie, J.; Wang, S.; Liu, Q.; Masliyah, J.; Zeng, H.; Xu, Z. *J. Phys. Chem. C* **2011**, *115*, 16043–16051.

- (9) Schramm, L. L. *Emulsions: fundamentals and applications in the petroleum industry*; American Chemical Society: Washington, DC, 1992.
- (10) Myers, D. *Surfactant Science and Technology*, 3rd ed.; Wiley-VCH: Weinheim, Germany, 2005.
- (11) Gafonova, O. V.; Yarranton, H. W. *J. Colloid Interface Sci.* **2001**, *241*, 469–478.
- (12) Schramm, L. L. *Surfactants: fundamentals and applications in the petroleum industry*; Cambridge University Press: New York, 2000.
- (13) Yang, X.; Hamza, H.; Czarnecki, J. *Energy Fuels* **2004**, *18*, 770–777.
- (14) Yarranton, H. W.; Hussein, H.; Masliyah, J. H. *J. Colloid Interface Sci.* **2000**, *228*, 52–63.
- (15) Buenrostro-Gonzalez, E.; Groenzin, H.; Lira-Galeana, C.; Mullins, O. C. *Energy Fuels* **2001**, *15*, 972–978.
- (16) Poteau, S.; Argillier, J. F.; Langevin, D.; Pincet, F.; Perez, E. *Energy Fuels* **2005**, *19*, 1337–1341.
- (17) Zhang, L. Y.; Breen, P.; Xu, Z.; Masliyah, J. H. *Energy Fuels* **2007**, *21*, 274–285.
- (18) Liu, J.; Zhang, L.; Xu, Z.; Masliyah, J. *Langmuir* **2006**, *22*, 1485–1492.
- (19) Wang, S.; Liu, J.; Zhang, L.; Masliyah, J.; Xu, Z. *Langmuir* **2009**, *26*, 183–190.
- (20) Sheremata, J. M.; Gray, M. R.; Dettman, H. D.; McCaffrey, W. C. *Energy Fuels* **2004**, *18*, 1377–1384.
- (21) Boek, E. S.; Yakovlev, D. S.; Headen, T. F. *Energ Fuels* **2009**, *23*, 1209–1219.
- (22) Mullins, O. C.; Sheu, E. Y. *Structures and dynamics of asphaltenes*; Plenum Press: New York, 1998.
- (23) Liu, J.; Xu, Z.; Masliyah, J. *Can. J. Chem. Eng.* **2004**, *82*, 655–666.
- (24) Liu, J.; Xu, Z.; Masliyah, J. *Colloids Surf. A* **2005**, *260*, 217–228.
- (25) Wang, S.; Liu, J.; Zhang, L.; Xu, Z.; Masliyah, J. *Energy Fuels* **2008**, *23*, 862–869.
- (26) Wang, J.; van der Tuuk Opedal, N.; Lu, Q.; Xu, Z.; Zeng, H.; Sjöblom, J. *Energy Fuels* **2011**, *26*, 2591–2599.
- (27) Nordgård, E. L.; Landsem, E.; Sjöblom, J. *Langmuir* **2008**, *24*, 8742–8751.
- (28) Nordgård, E. L.; Sjöblom, J. *J. Dispersion Sci. Technol.* **2008**, *29*, 1114–1122.
- (29) Nordgård, E. L.; Sørland, G.; Sjöblom, J. *Langmuir* **2009**, *26*, 2352–2360.
- (30) Rogel, E. *Langmuir* **2002**, *18*, 1928–1937.
- (31) Gawrys, K. L.; Spiecker, P. M.; Kilpatrick, P. K. *Pet. Sci. Technol.* **2003**, *21*, 461–489.
- (32) Zeng, H.; Pesika, N.; Tian, Y.; Zhao, B.; Chen, Y.; Tirrell, M.; Turner, K. L.; Israelachvili, J. N. *Langmuir* **2009**, *25*, 7486–7495.
- (33) Zeng, H.; Tian, Y.; Anderson, T. H.; Tirrell, M.; Israelachvili, J. N. *Langmuir* **2008**, *24*, 1173–1182.
- (34) Zeng, H.; Zhao, B.; Israelachvili, J. N.; Tirrell, M. *Macromolecules* **2009**, *43*, 538–542.
- (35) Teng, F.; Zeng, H.; Liu, Q. *J. Phys. Chem. C* **2011**, *115*, 17485–17494.
- (36) Hwang, D. S.; Zeng, H. B.; Masic, A.; Harrington, M. J.; Israelachvili, J. N.; Waite, J. H. *J. Biol. Chem.* **2010**, *285*, 25850–25858.
- (37) Zeng, H. B.; Hwang, D. S.; Israelachvili, J. N.; Waite, J. H. *Proc. Natl. Acad. Sci. U.S.A.* **2010**, *107*, 12850–12853.
- (38) Zeng, H. B.; Maeda, N.; Chen, N. H.; Tirrell, M.; Israelachvili, J. *Macromolecules* **2006**, *39*, 2350–2363.
- (39) Zeng, H. B.; Tirrell, M.; Israelachvili, J. *J. Adhesion* **2006**, *82*, 933–943.
- (40) Israelachvili, J.; Tabor, D. *Proc. R. Soc. London, A* **1972**, *331*, 19.
- (41) Israelachvili, J. N.; Adams, G. E. *J. Chem. Soc., Faraday Trans. 1* **1978**, *74*, 975–1001.
- (42) Tabor, D.; Winterton, R. *Proc. R. Soc. London, A* **1969**, *312*, 435–450.
- (43) Zeng, H. B.; Zhao, B. X.; Tian, Y.; Tirrell, M.; Leal, L. G.; Israelachvili, J. N. *Soft Matter* **2007**, *3*, 88–93.
- (44) De Gennes, P. *Adv. Colloid Interface Sci.* **1987**, *27*, 189–209.
- (45) [http://engineering.tufts.edu/microfab/index\\_files/SOP/PiranhaClean\\_SOP.pdf](http://engineering.tufts.edu/microfab/index_files/SOP/PiranhaClean_SOP.pdf).
- (46) Wenzel, R. N. *J. Phys. Colloid Chem.* **1949**, *53*, 1466–1467.
- (47) Stukan, M. R.; Ligneul, P.; Crawshaw, J. P.; Boek, E. S. *Langmuir* **2010**, *26*, 13342–13352.
- (48) Zhao, H. Y.; Bhattacharjee, S.; Chow, R.; Wallace, D.; Masliyah, J. H.; Xu, Z. H. *Langmuir* **2008**, *24*, 12899–12910.
- (49) Brückner, R. *Advanced organic chemistry: reaction mechanisms*; Academic Press: New York, 2002.
- (50) Derjaguin, B.; Churaev, N. *J. Colloid Interface Sci.* **1974**, *49*, 249–255.
- (51) Israelachvili, J. N. *Intermolecular and surface forces*, 3rd ed.; Academic Press: Waltham, MA, 2011.
- (52) da Silva, M. A. S.; Pinheiro, S. O.; Francisco, T. S.; da Silva, F. O. N.; Batista, A. A.; Ellena, J.; Carvalho, I. M. M. *J. Braz. Chem. Soc.* **2010**, *21*, 1754–1759.
- (53) Lide, D. R. *CRC handbook of chemistry and physics: a ready-reference book of chemical and physical data*; CRC Press: Boca Raton, FL, 2004.
- (54) Faghihnejad, A.; Zeng, H. B. *Soft Matter* **2012**, *8*, 2746–2759.
- (55) Christenson, H. K.; Claesson, P. M. *Adv. Colloid Interface* **2001**, *91*, 391–436.
- (56) Headen, T. F.; Boek, E. S. *Energy Fuels* **2011**, *25*, 499–502.